Time-dependent response of dissipative electron systems

Jean Christophe Tremblay,* Pascal Krause, Tillmann Klamroth, and Peter Saalfrank
Institut für Chemie, Universität Potsdam, Karl-Liebknecht-Straße 24-25, D-14476 Potsdam-Golm, Germany
(Received 22 March 2010; published 23 June 2010)

We present a systematic study of the influence of energy and phase relaxation on dynamic polarizability simulations in the linear response regime. The nonperturbative approach is based on explicit electron dynamics using short laser pulses of low intensities. To include environmental effects on the property calculation, we use the time-dependent configuration-interaction method in its reduced density matrix formulation. Both energy dissipation and nonlocal pure dephasing are included. The explicit treatment of time-resolved electron dynamics gives access to the phase shift between the electric field and the induced dipole moment, which can be used to define a useful uncertainty measure for the dynamic polarizability. The nonperturbative treatment is compared to perturbation theory expressions, as applied to a simple model system, the rigid H_2 molecule. It is shown that both approaches are equivalent for low field intensities, but the time-dependent treatment provides complementary information on the phase of the induced dipole moment, which allows for the definition of an uncertainty associated with the computation of the dynamic polarizability in the linear response regime.

DOI: 10.1103/PhysRevA.81.063420 PACS number(s): 33.15.Kr, 33.80.−b, 31.15.vn

I. INTRODUCTION

In recent years, ultrafast correlated electron dynamics has attracted increasing interest from both the experimental and the theoretical communities. The latest developments in subfemtosecond laser technology now make it possible to study and control the motion of electrons *in situ* using pulses only a few cycles or even less than one cycle long [1–6]. Although the literature on the topic was rather sparse until the end of the last millenium [7–11], an impressive body of work has been produced by theoreticians around the world over the past decade (see, for example, Refs. [12–36] and the numerous references therein).

Among the different approaches available emerges a family of methods based on wave-function expansions. These range from time-dependent Hartree-Fock [7], to time-dependent configuration-interaction (TDCI) [16,37], to time-dependent complete active space self-consistent field (CASSCF) (or multiconfiguration time-dependent Hartree-Fock) [18,23] methods. The latter two methods offer the great advantage that the dynamics, governed by the electronic Schödinger equation, can be, in principle, improved systematically toward its exact solution. In their original form, only isolated systems can be studied with those approaches since no interaction with the environment is explicitly included in the theoretical treatment.

To treat the environmental effects, we have proposed an extension of the TDCI method based on the reduced density matrix formulation, called ρ-TDCI in the following [38]. Energy transfer between the system and the environment, as well as nonlocal pure dephasing, are included in the dynamics using Lindblad dynamical semigroup formalism [39–44]. The method was applied to study intramolecular charge transfers and to control selective excitations using short, intense laser pulses in the linear molecule LiCN [38,45].

In a recent study [25], the dissipation-free TDCI method was used to compute molecular response properties in a time-dependent framework. It is the purpose of this article to extend the range of applications of ρ-TDCI to the study of linear response properties, with particular emphasis on the dynamic polarizability. To characterize this property, a static approach based on a pole and residues analysis has been introduced by Olsen and Jørgensen [46] and is nowadays widely appreciated. They provide a complementary picture to the sum-over-states expressions stemming from time-dependent perturbation theory [47–49]. These methods present singularities of the dynamic polarizability close to the resonance energies. To avoid this problem, a typical solution is to include a phenomenological damping parameter in the perturbation theory expressions [50–52]. Alternatively, Norman and co-workers [53,54] proposed a self-consistent formulation of the response equations based on the Ehrenfest theorem. Jørgensen and co-workers [55,56] also proposed a related model in terms of complex quasienergy, including a lifetime broadening parameter. The time-dependent density functional community also came up with an approach for including the effects of finite lifetime on linear response calculations [57,58]. All these methods used a simple phenomenological lifetime broadening constant for all electronic states.

We propose using the TDCI for open-system density matrix to study the effect of energy and phase relaxation on the dynamic polarizability in a time-dependent context. The propagation of the electronic density matrix in real time allows us to treat the response of the molecule to perturbations of arbitrary strength, beyond perturbation theory. State-resolved relaxation rates for explicitely correlated electron dynamics of a small molecule in a dissipative environment are determined as Einstein coefficients for spontaneous emission, with an empirical scaling factor to account for accelerated relaxation, for example, close to a metal surface or another electron-rich medium. The coupling strength of the system to the bath, and hence the energy broadening of the different electronic states, is varied systematically to mimic the effect of weakly to strongly coupled environments on the time-dependent induced dipole moment. To assess the quality of our method, we compare the nonperturbative treatment with existing

*jean.c.tremblay@gmail.com

sum-over-state expressions for the dynamic polarizability tensor. As a test case, the method is applied to H_2, but application to much larger systems is straightforward.

II. THEORY

A. Time-dependent configuration interaction for open systems

In the following, we use the TDCI approach [16] in its density matrix formulation [38] (ρ-TDCI) to compute the response properties of a small molecule, hereafter called the subsystem, in a dissipative environment. This is done by explicitly studying the evolution of the subsystem reduced density matrix under the influence of a time-dependent electric field. The time evolution of the density operator under the influence of a vectorial electric field $\underline{F}(t)$ obeys the Liouville-von Neumann equation, which is given in the semiclassical dipole approximation by

$$\frac{\partial\hat{\rho}(t)}{\partial t} = -i[\hat{H}_0,\hat{\rho}(t)] + i\sum_{q=x,y,z} F_q(t)[\hat{\mu}_q,\hat{\rho}(t)] + \mathcal{L}_D\hat{\rho}(t), \tag{1}$$

where $\hat{H}_0 = -\frac{1}{2}\sum_{i=1}^{N}\Delta_i + \sum_{i=1}^{N}\sum_{j<i}^{N}\frac{1}{|\underline{r}_i-\underline{r}_j|} - \sum_{i=1}^{N}\sum_{A=1}^{N_A}\frac{Z_A}{|\underline{r}_i-\underline{R}_A|}$ is the field-free electronic Hamiltonian for a system with N electrons and N_A nuclei. Further, $\hat{\mu}_q$ is the q^{th} component of the subsystem dipole operator [$\underline{\hat{\mu}} = -\sum_{i=1}^{N}\underline{r}_i + \sum_{A=1}^{N_A} Z_A\underline{R}_A = (\hat{\mu}_x,\hat{\mu}_y,\hat{\mu}_z)$], and $\mathcal{L}_D$ is the dissipative Liouvillian superoperator accounting for energy and phase relaxation (see later in this article). The single-electron kinetic energy $-\frac{1}{2}\Delta_i$, the position $\underline{r}_i$ of electron i, and the position $\underline{R}_A$ of nucleus A with charge Z_A are given in atomic units.

The standard configuration interaction singles (CIS) methodology can be used to solve the unperturbed electronic eigenvalue problem $\hat{H}_0\Psi_i = E_i\Psi_i$. As a first step, spatial orbitals are computed at the restricted Hartree-Fock level using the ground-state Slater determinant, Ψ_0^{HF}. A basis of singly excited configurations, Ψ_r^a, is then used to represent the full-dimensional subsystem electronic Hamiltonian. These configurations are generated by exciting one electron from occupied orbitals a to unoccupied orbitals r. In the present work we focus on singlet states and only the associated excited configurations, ${}^1\Psi_a^r = 1/\sqrt{2}(\Psi_a^r + \Psi_{\bar{a}}^{\bar{r}})$ ($\{a,r\}$ refer to α and $\{\bar{a},\bar{r}\}$ to β spin orbitals), are considered in the calculations. In that basis the electronic Hamiltonian matrix is then diagonalized to yield the CIS energies, E_i^{CIS}, and wave functions, Ψ_i. The CIS energies can be, for example, further corrected perturbatively by inclusion of double excitations, yielding CIS(D) energies $E_i^{\mathrm{CIS(D)}} = E_i^{\mathrm{CIS}} + E_i^{(\mathrm{D})}$, where $E_i^{(\mathrm{D})}$ is defined in a previous article [24,59]. The ground-state energy at this level, $E_0^{\mathrm{CIS(D)}}$, corresponds to the MP2 energy, E_0^{MP2}, whereas E_0^{CIS} is uncorrelated, giving the Hartree-Fock ground state, E_0^{HF}. The CIS(D) level of *ab initio* theory shall be used in the remainder of the article but could be improved in principle.

Using the CI eigenfunctions and energies we can represent compactly the subsystem reduced density operator. The direct integration of Eq. (1) is particularly efficient in the interaction picture [38], that is, if we perform the transformation $\hat{\rho}(t) = e^{i\hat{H}_0t/\hbar}\hat{\rho}^I(t)e^{-i\hat{H}_0t/\hbar}$. In the basis of the CI eigenstates, the equations of motion for the reduced density operator have a particularly simple form

$$\frac{d\rho_{mn}^I}{dt} = \frac{i}{\hbar}\sum_{q=x,y,z} F_q(t)\sum_{j=1}^{S}\left[e^{-i\omega_{mj}t}\mu_{mj}^{(q)}\rho_{jn}^I - e^{-i\omega_{jn}t}\rho_{mj}^I\hat{\mu}_{jn}^{(q)}\right] + e^{-i\omega_{mn}t}\langle\Psi_m|\mathcal{L}_D\hat{\rho}|\Psi_n\rangle, \tag{2}$$

where S is the number of CI eigenstates and $\hbar\omega_{mn} = E_m^{\mathrm{CI}} - E_n^{\mathrm{CI}}$ the energy difference between states $|\Psi_m\rangle$ and $|\Psi_n\rangle$, ρ_{mn}^I is the $\{m,n\}$ element of the density matrix in the interaction picture and $\mu_{mn}^{(q)} = \langle\Psi_m|\hat{\mu}_q|\Psi_n\rangle$ is the associated dipole matrix element along orientation q. In all our applications the equations of motion are solved numerically using a Cash-Karp Runge-Kutta integrator [38,60,61].

B. Dissipation model

To treat the energy and phase relaxation, we use the semigroup formalism introduced by Kossakowski and coworkers [40,41]. In particular, we use here the Lindblad form [39], which ensures semipositivy of the reduced density matrix. This allows interpretation of the diagonal elements of the reduced density matrix in the CI eigenstates basis as populations of these zeroth-order states. To simulate the effect of energy relaxation in an electron-rich environment such as a metal surface, we make the standard choice of using upward/downward projectors [38,42]. For treating the so-called "pure dephasing," the nonlocal contributions can be obtained by defining the Lindblad operators as the subsystem Hamiltonian scaled to fit the typical order of magnitude in the energy spectrum [42]. In the basis of the subsystem eigenstates, the matrix elements of the dissipative Liouvillian including both aforementioned contributions are given by [38]

$$\langle\Psi_n|\mathcal{L}_D\hat{\rho}|\Psi_n\rangle = \sum_{j=1}^{S}(\Gamma_{j\to n}\rho_{jj} - \Gamma_{n\to j}\rho_{nn}), \tag{3}$$

$$\langle\Psi_m|\mathcal{L}_D\hat{\rho}|\Psi_n\rangle = -\frac{1}{2}\sum_{j=1}^{S}(\Gamma_{m\to j} + \Gamma_{n\to j})\rho_{mn} - \gamma_{mn}^*\rho_{mn} \quad \text{for } m\neq n. \tag{4}$$

Here $\Gamma_{m\to n}$ is the transition rate between states $|\Psi_m\rangle$ and $|\Psi_n\rangle$ and γ_{mn}^* is the pure dephasing rate.

The downward transition rates are simply obtained by scaling the Einstein coefficients for spontaneous emission as (in atomic units)

$$\Gamma_{m\to n} = A\frac{4|\mu_{mn}^{\mathrm{tot}}|^2}{3c^3}\omega_{mn}^3. \tag{5}$$

Here c is the speed of light and $|\mu_{mn}^{\mathrm{tot}}|^2 = \sum_{q=x,y,z}|\langle\psi_m|\mu^{(q)}|\psi_n\rangle|^2$ the total transition dipole moment. The scaling factor A is chosen to mimic the presence of an arbitrary dissipative medium and reduces to the refractive index in vacuum ($A = 1$). The scaling factor can thus be interpreted as a phenomenological refractive index in the environment of interest. Upward transitions are forbidden at zero temperature, which is assumed here.

For the pure dephasing rates, we find a quadratic dependence on the energy difference, as suggested elsewhere [40,41,43,44],

$$\gamma^*_{mn} = B\gamma^*\omega^2_{mn}, \tag{6}$$

where B is an arbitrary positive constant that we shall vary to evaluate the effect of dephasing on the properties of interest. For the general constant γ^*, the convenient choice $\gamma^* = \Gamma_{1\to 0}\omega_{10}^{-2}$ has been assumed so that the pure dephasing rate is equal to the energy relaxation rate for the $1 \to 0$ transition when we set $B = 1$. For a more detailed discussion of the ρ-TDCI methodology and the present dissipation model, the reader is referred to Refs. [38,45].

C. Nonperturbative linear response calculations

The electron cloud around a molecule can be distorted by the presence of an external electric field, $\underline{F}(t)$. Polarizability is defined as the capacity of the electron density to undergo deformation under the influence of the external field, inducing a dipole moment. The component along coordinate q ($q = x,y,z$) of the induced dipole moment can be written in the general form

$$\mu_{\mathrm{ind},q} = \sum_{q'} \alpha_{qq'}F_{q'} + \frac{1}{2}\sum_{q'q''}\beta_{qq'q''}F_{q'}F_{q''} + \frac{1}{3!}\sum_{q'q''q'''}\gamma_{qq'q''q'''}F_{q'}F_{q''}F_{q'''} + \cdots, \tag{7}$$

where F_q is the qth component of the electric field, $\alpha_{qq'}$ is the $\{q,q'\}$th element of the polarizability tensor, and $\beta_{qq'q''}$ and $\gamma_{qq'q''q'''}$ are elements of the first and second hyperpolarizability tensor. These quantities are frequency dependent and depend on frequency-dependent electric fields, for example, $\alpha_{qq'} \to \alpha_{qq'}(-\omega;\omega)$. Using a low-intensity electric field, the response of the electron density can be considered linear to a good approximation and only the first term in Eq. (7) remains of interest. It must be stressed that the explicitly time-dependent correlated electron dynamics approach proposed here is an exact treatment and contains the response function to all orders.

It was shown previously [25] that, in the linear response, the polarizability tensor $\underline{\underline{\alpha}}$ can be probed by looking at the indiviual components of the dipole moment induced by nonresonant subpicosecond polarized laser pulses. Let us consider the simple case where the probed molecule is put in a low-intensity z-polarized electric field of the form

$$F_z(t;\omega) = F_{0,z}\sin^2\left(\frac{\pi t}{2t_m}\right)\cos[\omega(t-t_m)]; \quad 0 \leqslant t \leqslant t_m, \tag{8}$$

where $F_{0,z}$ is the field amplitude and t_m is the center of the pulse. The probe molecule to be considered in what follows is H_2, for which we fix the orientation along the z axis. The real part of the zz dynamic polarizability component at time t can be expressed as a function of the laser carrier frequency ω using the relation

$$\alpha^{(R)}_{zz}(t;\omega) = \frac{\mu_z(t)}{F_z(t;\omega)}. \tag{9}$$

In the following, the quantity $\alpha^{(R)}_{zz}(t;\omega)$ is evaluated at the field maximum (t_m) if not stated otherwise. Further, the imaginary part of the polarizability tensor, from which one can extract the absorption cross section, can be obtained from its real part using the Kramers-Kronig rule,

$$\alpha^{(I)}_{qq'}(-\omega;\omega) = \frac{-2\omega}{\pi}\int_0^\infty \frac{\alpha^{(R)}_{qq'}(-\omega';\omega')}{\omega'^2-\omega^2}d\omega'. \tag{10}$$

The quantity (9) can be interpreted as the Fourier transform of the associated polarizability tensor elements, say $\alpha^R_{zz}(-\omega;\omega)$. It is, in general, not possible, however, to perform the inverse Fourier transform of Eq. (9) to recover the true frequency dependence of the polarizability tensor. The latter presents poles in the frequency domain when the carrier frequency is chosen resonant with a transition energy of the system. In the time domain, this introduces a phase shift of the induced dipole moment, which lags the field by $\pi/2$ like in the case of a classical driven damped harmonic oscillator. The time at which one should evaluate the polarizability tensor is thus not rigorously defined, particularly at the transition energy. We could either use the value at the field maximum, for which the induced dipole is zero, or that at the maximum dipole, where the field vanishes and the polarizability diverges. We propose to use the difference in these two values as a measure of the uncertainty on the polarizability calculation,

$$\Delta\alpha^{(R)}_{zz}(\omega) = \left|\frac{\alpha^{(R)}_{zz}(t_m;\omega) - \alpha^{(R)}_{zz}(t_\mu;\omega)}{\alpha^{(R)}_{zz}(t_m;\omega)}\right|, \tag{11}$$

where t_m and t_μ are the time at which the field and the induced dipole moment reach their maximal value, respectively.

D. Other approaches to dissipative polarizability calculations

Time-dependent perturbation theory can also be used for computing dynamic polarizabilities. It was shown [48–52] that the real and imaginary parts of the qq' component of the polarizability tensor in a dissipative system can be computed using sum-over-states formulæ,

$$\begin{aligned}\alpha^{(R)}_{qq'}(-\omega;\omega) &= \sum_n\left[\frac{\langle 0|\mu_q|n\rangle\langle n|\mu_{q'}|0\rangle(\omega_{0n}-\omega)}{(\omega_{0n}-\omega)^2+\gamma^2_{n0}} + \frac{\langle 0|\mu_q|n\rangle\langle n|\mu_{q'}|0\rangle(\omega_{0n}+\omega)}{(\omega_{0n}+\omega)^2+\gamma^2_{n0}}\right],\\ \alpha^{(I)}_{qq'}(-\omega;\omega) &= \sum_n\gamma_{n0}\left[\frac{\langle 0|\mu_q|n\rangle\langle n|\mu_{q'}|0\rangle}{(\omega_{0n}-\omega)^2+\gamma^2_{n0}} - \frac{\langle 0|\mu_q|n\rangle\langle n|\mu_{q'}|0\rangle}{(\omega_{0n}+\omega)^2+\gamma^2_{n0}}\right],\end{aligned} \tag{12}$$

provided we have a model for describing the dissipation rates. The state-resolved energy-broadening constants γ_{n0} are defined in terms of the state-to-state relaxation rates as the total dephasing rate, $\gamma_{n0} = \frac{1}{2}\sum_i(\Gamma_{n\to i}+\Gamma_{0\to i}) + \gamma^*_{n0}$.

Since there is considerable uncertainty on the state-resolved energy-broadening parameters, a common assumption is to set them all to a constant, $\gamma_{n0} \to \gamma$, where γ can be interpreted as a phenomenological energy broadening, related to the system

lifetime and pure dephasing. Under this condition, Eqs. (12) simplify to

$$\alpha^{(R)}_{qq'}(-\omega;\omega) = \sum_n \left[\frac{\langle 0|\mu_q|n\rangle\langle n|\mu_{q'}|0\rangle(\omega_{0n}-\omega)}{(\omega_{0n}-\omega)^2+\gamma^2} + \frac{\langle 0|\mu_q|n\rangle\langle n|\mu_{q'}|0\rangle(\omega_{0n}+\omega)}{(\omega_{0n}+\omega)^2+\gamma^2}\right],$$
$$\alpha^{(I)}_{qq'}(-\omega;\omega) = \gamma \sum_n \left[\frac{\langle 0|\mu_q|n\rangle\langle n|\mu_{q'}|0\rangle}{(\omega_{0n}-\omega)^2+\gamma^2} - \frac{\langle 0|\mu_q|n\rangle\langle n|\mu_{q'}|0\rangle}{(\omega_{0n}+\omega)^2+\gamma^2}\right]. \quad (13)$$

These models were compared to dissipative time-dependent density functional calculation in a recent article by Jensen and co-workers [58] and are compared to the nonperturbative treatment in the following.

III. NUMERICAL SIMULATIONS

A. Time-dependent basis parameters

For our numerical simulations, we choose to study the dynamic polarizability of H_2. This model system has been a playground for theoreticians for a quite a long time already [62–65] and thus provides a good benchmark for our nonperturbative linear response simulations. We fixed the nuclear distance at its experimental value of $R_{HH} = 1.401 a_0$ and defined the z axis along the molecular axis. It is well-known that the dynamic polarizability is influenced by the nuclear motion [66], in particular for a small molecule like H_2 with an oscillation period below 10 fs. The fixed-nuclei approximation certainly represents a limitation of the present model. Fortunately, including the effect of nuclear motion on the dynamic polarizability tensor is straightforward. The idea is to calculate the dynamic polarizability tensor at different internuclear distances, R_{HH}, and then average according to the result on the initial vibrational wave function,

$$\alpha^{(R,I)}_{qq'}(t;\omega) = \sum_\nu P_\nu \int_0^\infty \psi^*_\nu(R_{HH})\alpha^{(R,I)}_{qq'}(t;\omega;R_{HH})\psi_\nu(R_{HH})dR_{HH}, \quad (14)$$

where ψ_ν is the νth vibrational eigenstate on the ground potential energy surface and P_ν is its Boltzmann weight. We prefer leaving the vibrational averaging aside to put the emphasis on the effects of energy and phase relaxation of the electronic states on a single-point calculation of the dynamic polarizability tensor.

Using Dunning's augmented correlation-consistent polarized valence quadruple ζ basis set [67,68], the 92 orbitals computed at the Hartree-Fock level were combined to form a full basis of singlet states. The wave functions were computed at the CIS level and the energies were corrected perturbatively to include the effect of double excitations. Figure 1 shows schematically the first few eigenenergies of H_2 obtained at the CIS(D) level of theory, classified according to the orientation of their transition dipole moment. The ionization potential,

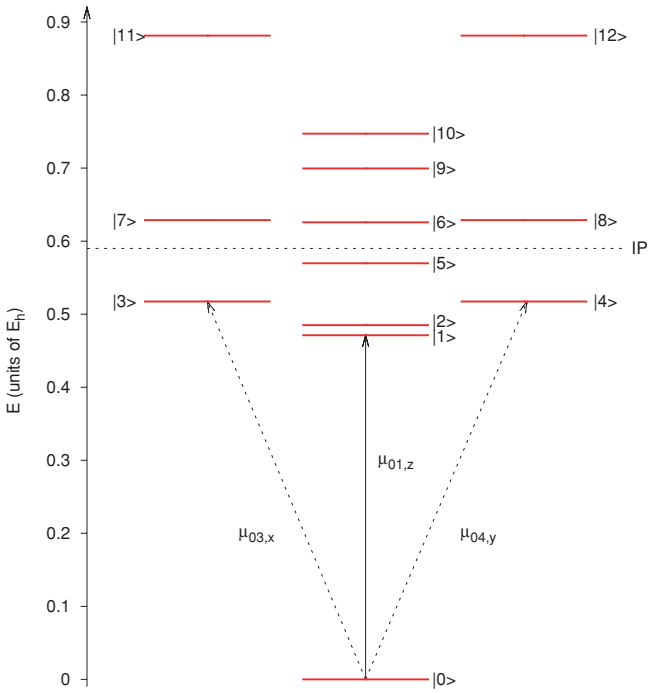

FIG. 1. (Color online) First few energy levels of H_2 computed at the CIS(D) level of theory using Dunning's aug-cc-pVQZ basis set. The states on the left (right) are accessible from the ground state using an x- (y-)polarized electric field, while the states in the middle are accessible using a z-polarized electric field. The ionization potential IP is at 0.594 45 E_h.

calculated from Koopmans' theorem, is at 0.594 45 E_h, just above state $|5\rangle$.

The basis size for the time-dependent calculation was tested for convergence. Whereas a minimal two-state basis appears sufficient for converging the dynamic polarizability curve close to the resonance energies, up to 60 states were included in the basis to achieve full convergence off resonance. These correspond to states below 4.69 Hartree, where there is coincidently a large gap of about 1 hartree in the CIS(D) energies. All calculations have been performed with the latter basis of 60 singlet states at the CIS(D) level.

The nonperturbative dynamic polarizability calculations in a time-dependent framework depend on the duration of the pulse used to measure the property. Throughout the article all calculations have been performed using z-polarized electric fields according to Eq. (8) with amplitude $F_{0,z} = 10^{-10} E_h/ea_0$. Figure 2 shows the effect of the pulse duration on the real part of the dynamic polarizability for the system with and without dissipation close to the first resonant transition. The pulse length was varied from 25 fs to 10 ps. In the top panel, which corresponds to the dissipation-free case, we see that the real dynamic polarizability along z is indeed greatly affected by the pulse length, as the linear response becomes larger close to the resonance for longer pulse.

This is an indication that, for very short pulses, the field and the response property are convoluted. In the inset the details of the real dynamic polarizability close to the resonance are better seen. With a pulse

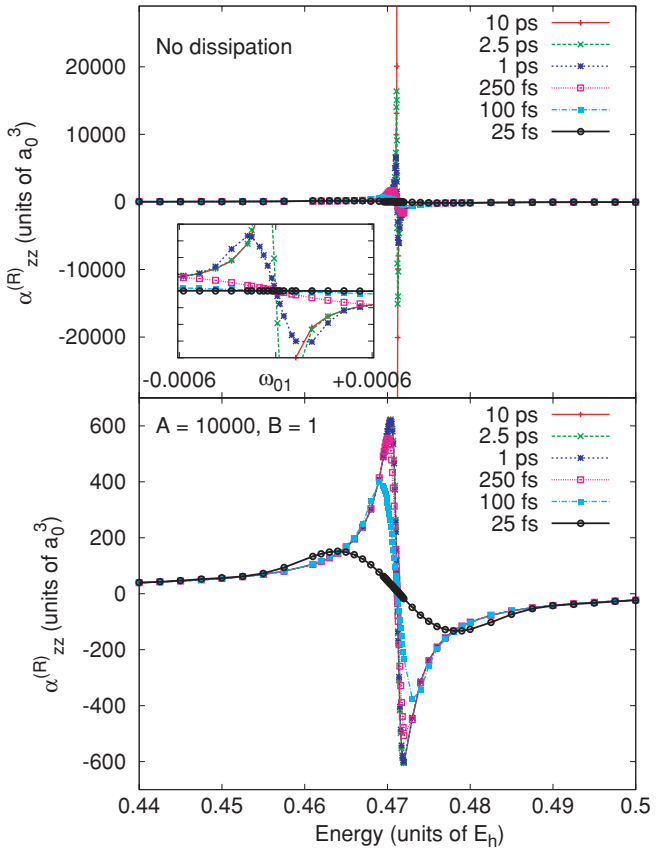

FIG. 2. (Color online) Effect of the pulse duration on the zz component of the dynamic polarizability tensor of H_2 close to the $0 \rightarrow 1$ transition computed using the ρ-TDCI method and a $\sin^2$ pulse with maximal amplitude 10^{-10} E_h/ea_0. The convolution of the field and the dynamic polarizability without and with ($A = 10^4$ and $B = 1$) dissipation is shown in the top and bottom panels, respectively. The signals obtained with the three longer pulses overlap in the bottom panel. In the inset, the detailed behavior close to the resonance point for the nondissipative system is shown.

of 1 ps, the response is similar to that obtained with longer pulses until ~0.5 millihartree about the transition energy.

In the bottom panel of Fig. 2, we see the effect of the pulse duration on a H_2 molecule placed in a strong dissipative environment. We use the model defined in Sec. II B, where the energy relaxation parameter A in Eq. (5) is set to 10^4 and the pure dephasing parameter B in Eq. (6) is set to 1. For theses parameter values, the effect of pure dephasing and energy relaxation are of comparable magnitude. Using this model, the lifetime of the first excited state is about $\tau_{1\rightarrow 0} = 1/\Gamma_{1\rightarrow 0} \simeq 43$ fs. As was the case for the nondissipative system, we can see that the dynamic polarizability is convoluted with the field for short pulse lengths. On the other hand, the simulation converges much more quickly as the duration of the pulse is increased. While almost converged at 250 fs, the simulations do not show any change for pulses longer than 1 ps. Thus, the polarizability is completely deconvoluted from the field for pulse durations on the order of a picosecond, and the remainder of the simulations have be done in this time regime.

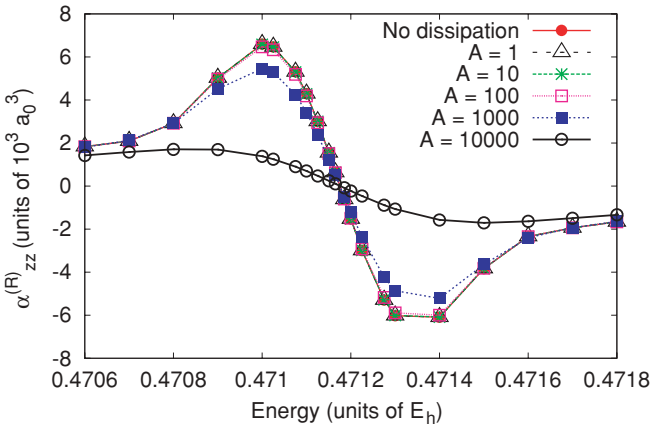

FIG. 3. (Color online) Effect of energy relaxation on the zz component of the dynamic polarizability tensor α_{zz} of H_2 close to the $0 \rightarrow 1$ transition computed using the ρ-TDCI method. A $\sin^2$ pulse of duration 1 ps and maximal amplitude 10^{-10} E_h/ea_0 was used for all calculations. The pure dephasing is set to $B = 0$.

B. Energy and phase relaxation

Figure 3 shows the effect of the strength of energy dissipation on the real part of the zz component of the dynamic polarizability tensor α_{zz} of H_2 close to the first transition energy at 0.471 175 E_h. The pure dephasing has first been neglected by setting $B = 0$ in Eq. (6). Each point in the figure represents a simulation using a 1-ps pulse defined by Eq. (8) for different frequencies ω. The real part of the polarizability tensor has been extracted at the field maximum, t_m, according to Eq. (9).

By increasing the constant A in our dissipation model, we can see the effect of energy relaxation becoming more important. For $A = 1$, representing coupling to the vacuum, the lifetime of the first excited state is on the order of 430 ps. Since we are using much shorter laser pulses, the dynamic polarizability is numerically equivalent to that without dissipation. For $A = 100$, which yields lifetimes on the same order as the laser pulse length, the dynamics begins to differ from that of the nondissipative system. Also, the field and the response do not appear to be convoluted anymore. The largest value of A corresponds to an electron-rich environment, such as the one found when the molecule is close to a metallic surface, in which case the dynamic polarizability is almost flat compared to the others. Interestingly, all the different dissipative environments yield a dynamic polarizability that crosses 0 exactly at the resonance energy. This stems from the phase shift between the induced dipole moment and the field, the former vanishing at the point in time at which the latter reaches its maximum for resonant excitation frequency.

Turning now our attention to the effect of nonlocal pure dephasing, we have studied environments for which the lifetime of the first subsystem excited state is, at most, of comparable magnitude as the laser pulse used for the simulation, here again chosen as 1 ps. Figure 4 shows the zz component of the real dynamic polarizability for the environments with parameter $A = 1000$ ($\tau_{1\rightarrow 0} = 430$ fs) and $A = 10^4$ ($\tau_{1\rightarrow 0} = 43$ fs). The relative contribution of pure dephasing with respect to energy dissipation was varied from

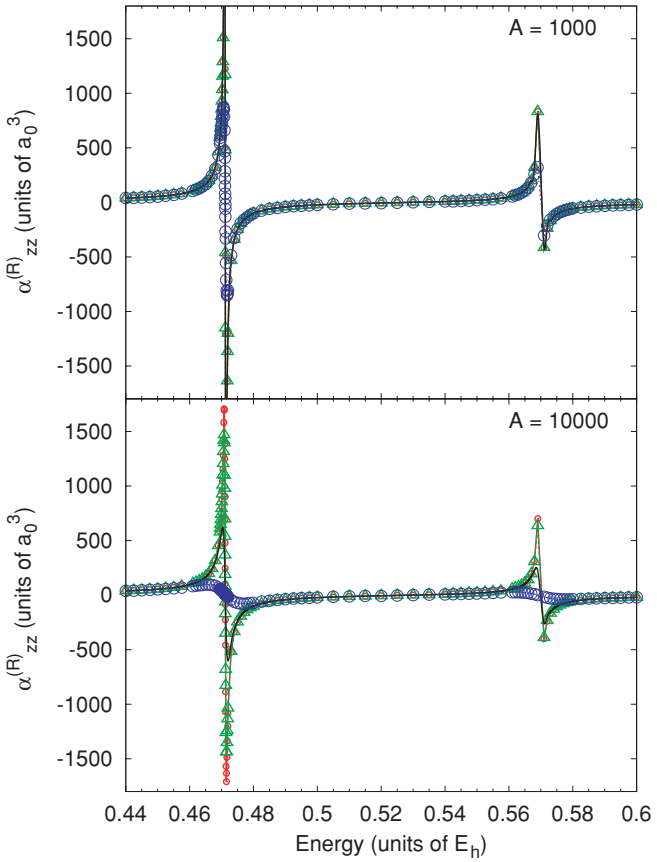

FIG. 4. (Color online) Effect of pure dephasing on the zz component of the dynamic polarizability tensor of H_2 for different energy relaxation rates, computed using the ρ-TDCI method and a $\sin^2$ pulse of duration 1 ps with maximal amplitude 10^{-10} E_h/ea_0. The red (gray) dotted line include no pure dephasing. The green (light gray) triangles, the black line line, and the blue (dark gray) circles are obtained by setting $B = \{0.1, 1.0, 10\}$, respectively.

inexistent ($B = 0$, small red circles) to small ($B = 0.1$, green triangles), to comparable in magnitude ($B = 1$, black solid line), to dominating ($B = 10$, large blue circles).

In the top panel, one can see that the first peak of the response is indeed affected by the nonlocal pure dephasing due to the environment, whereas the second resonant peak at $\hbar\omega_{05} = 0.569\,67 E_h$ seems less sensitive. Note that the transition at energy $\hbar\omega_{02} = 0.485\,04 E_h$ is not observed because the transition dipole moment is 10 orders of magnitude smaller than that associated with the two other transitions. The reduction of the dynamic polarizability amplitude close to the resonance energies with increasing pure dephasing is also seen for less dissipative environments. The effect becomes marginal when the lifetimes are much longer than the pulse duration, and thus the curves have not been shown here. The bottom panel shows the effect of pure dephasing on the polarizability of H_2 in an electron-rich environment (with $A = 10^4$). The response reduction is already visible when $B = 0.1$, and the polarizability becomes almost flat when pure dephasing dominates energy relaxation. Furthermore, we see that the second peak is apparently more affected by pure dephasing when energy dissipation is larger (compare top and bottom panels).

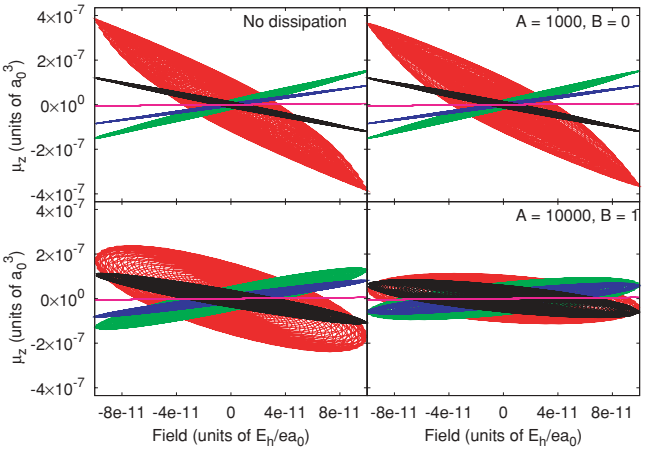

FIG. 5. (Color online) Kennlinien for H_2 using four different dissipation rates. A z-polarized $\sin^2$ pulse of duration 1 ps and maximal amplitude 10^{-10} E_h/ea_0 was used in all cases. The magenta (light gray) line, the blue (dark gray), the green (light gray), the red (gray, largest amplitude), and black (with negative slope) ellipsoids are obtained for fields with carrier frequency 0.4500, 0.4700, 0.4705, 0.4715, and 0.4720 E_h, respectively.

C. Time-dependent dipole and uncertainty assessment

To understand the behavior of the method and assess its reliability, it is important to look at what happens to the induced dipole moment as a function of time. As proposed in our previous article [25], one can look at the so-called *kennlinie* in the $\mu_z(t)$-$F_z(t;\omega)$ plane for different carrier frequencies. A kennlinie is simply a parametric plot of dependent variables, here the induced dipole and the electric field as a function of the time parameter. For different dissipative environments, they are shown in Fig. 5. The magenta lines represent excitations far from resonance, at $\hbar\omega = 0.4500 E_h$. For all dissipative environments, the kennlinie is almost a flat line and the induced dipole moment and the field are in phase, as expected. As one approaches the resonance energy at 0.471 175 E_h, the line starts to deform into an ellipse due to the increasing phase shift between the two quantities. The blue curve corresponds to a carrier frequency of $\hbar\omega = 0.4700 E_h$ and the green curve to $\hbar\omega = 0.4705 E_h$. From the two top panels we can see that the slope of the line bisecting the long axis of the ellipses is getting smaller as dissipation is turned on. This explains the decrease in the amplitude of the dynamic polarizability curve observed in Fig. 3. The very small change observed in the top two panels is due to the convolution of the field and the induced dipole moment for the nondissipative case.

Looking at the bottom left panel, where energy relaxation is now ten times faster than in the top right panel, we see that not only the slope of the bisector is getting smaller but also the ellipse is getting rounder. Thus, it seems that increasing energy relaxation will lead to larger phase shift between the induced dipole moment and the electric field. This is paralleled by the reduction of the real dynamic polarizability curve amplitude, as seen in Fig. 3. If one further adds the effect of nonlocal pure dephasing to the simulation, the kennlinien become even rounder and have an even flater slope. The increase in phase shift between field and dipole is reflected also in the reduction of the polarizability shown in Fig. 4. The last two curves

observed in Fig. 5 are obtained for carrier frequencies that are slightly above the resonance energy, at $0.4715E_h$ and $0.4720E_h$ for the red and blue curves, respectively. The same trends as previously discussed can be observed when the influence of energy relaxation and pure dephasing are turned on. The most interesting characteristic of these kennlinien is that the slope of their bisector is now negative, which can be easily justified by looking at Eq. (12).

Note that all the simulations discussed above are in the linear response regime, since no electronic transition takes place with such low-intensity pulses with carrier frequency far enough off resonance. The associated kennlinien are thus evolving smoothly in the $\mu_z(t)$-$F_z(t;\omega)$ plane. When the laser energy approaches the transition energy, a kink can be observed in the kennlinien for the nondissipative system, as shown in the top left panel of Fig. 6. The yellow, black, and red lines are kennlinien obtained for carrier frequencies $\hbar\omega = 0.4700E_h$, $\hbar\omega = 0.4709E_h$, and $\hbar\omega = 0.4710E_h$, respectively. The latter two are located just below the transition energy at 0.471 175 E_h. This kink has its origin in the transfer of an almost negligible amount of population to the first excited state, as can be seen from the top right panel of Fig. 6.

Far from resonance (yellow curve), the dipole moment increases as the field rises before going back to zero as the field is turned off. Closer to resonance (black curve), the induced dipole moment does not return completely to zero after the field is turned off. Small-amplitude oscillations are observed at the end of the pulse, which indicate the creation of an electronic wave packet. The population of the excited state remains very small, slightly above the numerical accuracy, but one should already consider that the simulation departs from the continuous-wave limit. This trend is even more pronounced when using a carrier frequency closer to the resonant transition, as can be seen from the red curve in the top right panel. When compared to the dissipative system, the behavior of the latter is much more regular. In the bottom left panel we can see the kennlinien for the same three carrier frequencies as the top panel for a system in a strong dissipative environment ($A = 10^4$). All three curves have a much smaller intensity than in the nondissipative case, and they have a much more regular ellipsoid shape. Looking at the bottom right panel, it is clear that there is no creation of an electronic wave packet in the dissipative environment. For all three energies, the induced dipole moment rises and falls with the field strength. The infinitesimal population that might be pumped up to the excited state is brought down to the ground state by energy relaxation. Thus, the associated kennlinie do not present any kink.

As seen from the kennlinien, both the electric field and the induced dipole moment are time-dependent quantities. Thus, the polarizability computed according to Eq. (9) will also depend on time. All polarizabilities presented in the present article have been chosen at the field maximum, because it is a well-defined quantity. In particular for carrier frequencies far off resonance, the polarizability at the field and at the induced dipole maximum is almost the same. On the other hand, the difference between the two values is much larger close to the resonance. As pointed out before, this has its origin in the phase shift of the two quantities, which is of $\pi/2$ for the resonant transition. The difference between the two values can be used as an uncertainty measure on the calculated polarizability, as proposed in Eq. (11). Figure 7 shows the uncertainty associated with the real part of the zz component of the dynamic polarizability tensor of H_2 in a strong dissipative environment ($A = 10^4$ and $B = 1$).

The top panel shows the polarizability and the associated uncertainty is shown in the bottom panel. The phase shift of the induced dipole moment with respect to the field is also shown in the bottom panel. As the carrier frequency gets close to the resonance, the latter rises to reach a maximum

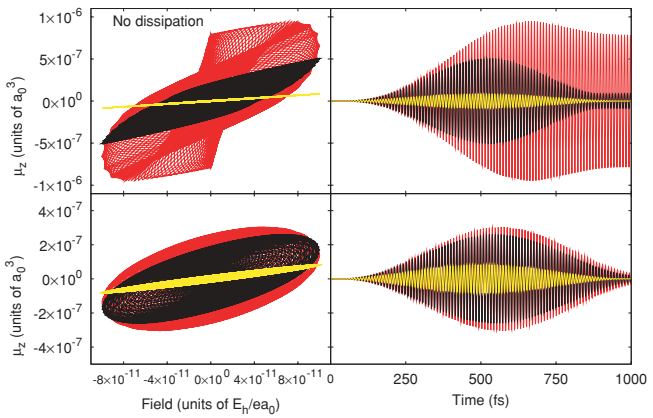

FIG. 6. (Color online) Effect of dissipation on the kennlinien for H_2 close to the resonant transition at 0.471 175 E_h obtained with a z-polarized $\sin^2$ pulse of duration 1 ps and maximal amplitude 10^{-10} E_h/ea_0. The associated time-dependent induced dipole moment is shown in the right panels. The yellow (light gray), black, and red (gray, largest amplitude) lines are associated with carrier frequency 0.4700, 0.4709, and 0.4710 E_h, respectively.

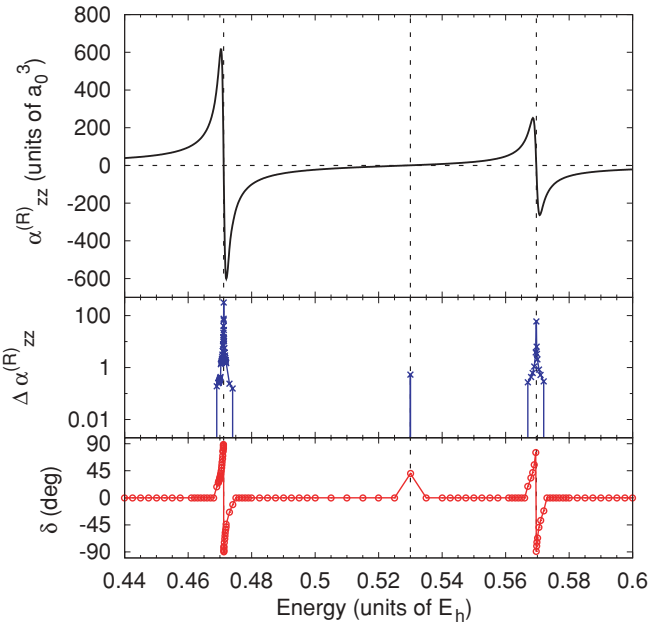

FIG. 7. (Color online) Uncertainty in the zz component of the dynamic polarizability tensor of H_2 according to Eq. (11). A z-polarized $\sin^2$ pulse of duration 1 ps and maximal amplitude 10^{-10} E_h/ea_0 was used. The lowest panel shows the phase shift δ of the induced dipole moment.

and falls after crossing the resonance. This is true for both the transitions at 0.471 175 E_h and 0.569 67 E_h, as shown by the vertical dotted lines. The relative uncertainty is found to be much larger than the polarizability value at these points. The third dotted line is there to illustrate that the uncertainty also increases slightly when the polarizability crosses zero. This is a numerical problem, since the relative uncertainty in Eq. (11) will diverge when the induced dipole moment crosses zero. The same numerical difficulty arises in the determination of the phase shift. In the bottom panel, we see an unphysical increase in the phase shift when the induced dipole crosses zero, which is purely of numerical origin. Note that the phase shift is not defined when the induced dipole moment strictly equals zero. Thus, the uncertainty measure we propose follows the behavior one would intuitively expect.

D. Comparison with the perturbative treatment

It is possible to obtain both the real and imaginary parts of the polarizability tensor using time-dependent perturbation theory. Figure 8 compares the real part of the polarizability obtained using the sum-over-states expressions (13) and (12) with the nonperturbative treatment. The green line represent the system without dissipation, for which one can clearly see that the polarizability diverges at both resonant transition energies. The three other lines have been computed for a strong dissipative environment ($A = 10^4$ and $B = 1$). The dashed blue line refers to the standard formula (13) using constant energy broadening, and the black line refers to Eq. (12), for which state-to-state transition rates were computed using the model exposed in Sec. II B. The constant energy broadening is chosen equal to the transition rate from the first excited to the ground state. The red dotted line was obtained using ρ-TDCI with the same set of state-resolved transition rates as for the perturbative approach.

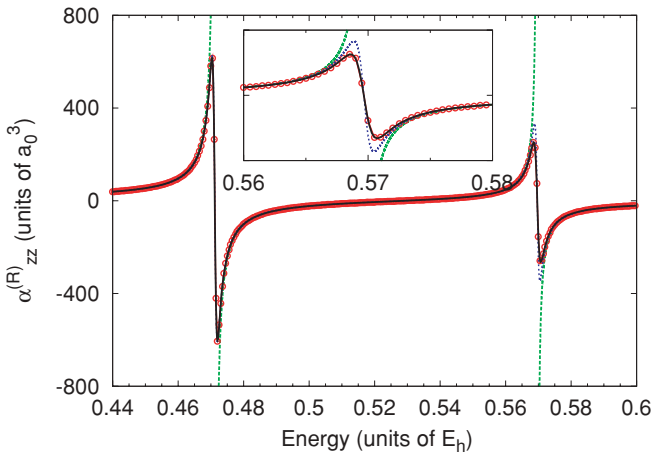

FIG. 8. (Color online) Comparison of the real part zz component of the dynamic polarizability tensor of H_2 obtained using different methods. The dashed green (light gray) line is obtained using sum-over-states perturbation theory without dissipation [Eq. (13) with $\gamma = 0$]. The dotted blue (dark gray) line is obtained using the sum-over-states model with constant dissipative rate [Eq. (13)]. The red (gray) line with large circles is obtained using the refined SOS-PT model of Eq. (12). The solid black line is computed with ρ-TDCI, using a $\sin^2$ pulse of duration 1 ps with maximal amplitude 10^{-10} E_h/ea_0. The latter two lines coincide with each other. The detailed behavior of the dynamic polarizability for the $0 \rightarrow 5$ transition is shown in the inset.

It can be seen that all different methods yield quantitatively the same dynamic polarizability when the electric field is chosen off resonance. Interestingly, this is valid for both the dissipative and nondissipative environments. Thus, the effects of dissipation are only seen in the vicinity of the resonances, where we already saw that energy relaxation prevents the creation of an electronic wave packet. In the inset, we can see the behavior of the real polarizability around the second excited state accessible using a z-polarized electric pulse. Although the perturbation theory for the nondissipative system diverges (green dashed curve), all other curves reach a maximum slightly below the resonance and cross the zero at the transition energy before reaching a minimum at an energy above the resonance. The profile is in all cases symmetric about the resonant energy. The perturbation theory yields a larger curve amplitude than the refined formula (12). This is not to be seen from the lower energy transition, where both perturbation theory expressions and the explicitly time-dependent treatment are equal by construction. At higher energy, dissipation is more efficient and thus the state-resolved energy broadening ($\gamma^*_{5\rightarrow 0} = 1.048 \times 10^{-3} E_h \hbar^{-1}$) becomes larger than the constant energy-broadening parameter ($\gamma = 8.005 \times 10^{-4} E_h \hbar^{-1}$) used in Eq. (13).

The nonperturbative treatment follows both other methods, but the curve has somewhat less amplitude than the one computed using expression (13). The result is numerically equivalent to the state-resolved formula (12), as can be seen from the figure. This indicates that, although the sum-over-states perturbation theory is only strictly valid far from resonance where the perturbation to the zeroth-order system is small, the field amplitude remains so small that the inclusion of state-resolved energy-broadening constants to the perturbation theory suffice to reproduce the numerical behavior of the dynamic polarizability. Note that the perturbation theory expression does not include any information about the phase shift of the induced dipole moment. As seen in the previous section, this phase shift leads to an uncertainty in the definition of the time at which one should evaluate the dynamic polarizability. From Fig. 8, it can clearly be seen that the perturbation theory expression is based on the evaluation of the linear response quantity at the field maximum. This is why perturbation theory always yields a definite value. This arbitrary time definition can be avoided by computing the dynamic polarizability using the time-dependent correlated electron dissipative dynamics approach proposed here. This does not only give access to the phase shift of the induced dipole moment, but also includes the effect of the perturbation to all orders in the field expansion for arbitrary field strengths and field envelope functions (cf. Fig. 2).

Figure 9 shows the imaginary part of the dynamic polarizability for the same strong dissipative environment as in Fig. 8. The green and blue curves refer as before to the simple and refined perturbation theory expressions, respectively. The red curve is obtained by transforming the nonperturbative real polarizability using the Kramers-Kronig rule [Eq. (10)]. The latter is almost in perfect agreement with the result obtained with the state-resolved perturbation theory [Eq. (12)]. Both

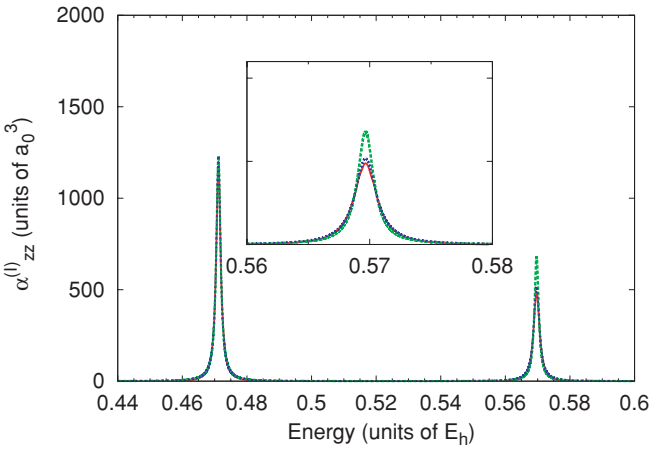

FIG. 9. (Color online) Comparison of the imaginary part zz component of the dynamic polarizability tensor of H_2 obtained using different methods. The solid red (gray) line is obtained from the real part using the Kramers-Kronig rule. The green (light gray) line is obtained using the sum-over-states model with constant dissipative rate. The dashed blue (dark gray) line is obtained using the refined SOS-PT model of Eq. (12). The detailed behavior of the dynamic polarizability for the $0 \rightarrow 5$ transition is shown in the inset.

have a smaller amplitude and have a larger width than the constant rate perturbative calculation [Eq. (13)]. This can be rationalized on the basis that also the real polarizability is of larger magnitude in the latter cases. In the inset we see that the Kramers-Kronig transformation of the real polarizability yield a curve amplitude that is slightly smaller than the state-resolved perturbative treatments. This is due to small inaccuracies in the numerical integral, since both methods yield the same real dynamic polarizability and should thus have the same imaginary counterpart, provided there is an analytical expression for the real part.

IV. CONCLUSION

In conclusion, we have studied the effects of finite electronic lifetimes on the dynamic polarizability of a simple molecule, H_2, in a dissipative environment. The ρ-TDCI method made it possible to investigate the linear response property in a time-resolved correlated electron dynamics framework. Energy relaxation and pure dephasing were included using the Lindblad semigroup formalism. The state-to-state transition rates were computed using a scaled spontaneous emission approach, for which the parameters were varied systematically in order to simulate the effect of electron-rich media.

Ultrashort laser pulses of various durations revealed the convolution of the field and the polarizability close to the resonant transition energies. It appeared that dissipation reduces significantly the degree of convolution of the property and the field. Both energy relaxation and pure dephasing were studied separately and induced a reduction in the dynamic polarizability amplitude, as well as a slight broadening of the peaks. Far off resonance the kennlinien [that is, the parametric plot in the $\mu_z(t)$-$F_z(t;\omega)$ plane] showed rounder ellipsoids with smaller induced dipole moment with increasing dissipative rate. In the absence of dissipation, creation of an electronic wave packet is observed close to the resonance energy even at very low field intensity; a kink is seen in the kennlinien. This effect is masked by dissipation and the kennlinien remain well-behaved near resonance. The ambiguity associated with the time at which the dynamic polarizability should be computed was used to define a simple measure of uncertainty. This provides more insight into the relative phase behavior of the dynamic polarizability, in particular close to resonant transitions.

Finally, comparison of the perturbative and nonperturbative treatments revealed that, for the weak fields considered here, both methods are very similar far off resonance for the real component of the polarizability tensor. Some discrepancies arise close to resonances for the model using constant energy broadening, where the state lifetimes are not properly treated. The signal amplitude proved significantly lower using the state-to-state lifetime model proposed earlier, computed either with the state-resolved perturbation theory expression or our ultrafast correlated electron dissipative dynamics method. The time-dependent approach allows for an accurate description of the phase of the induced dipole moment as well as containing the field induced perturbation of the electronic density to all orders exactly. This picture offers complementary information to the frequency-domain approaches, represented here by the perturbation theory expressions.

Although the ρ-TDCI method is applied to a simple test case in the present article, it could be used to characterize many other systems of current interest. These range from the response properties of quantum dots with potential application to qubits to the ultrashort dynamics in molecular electronic devices or the electron scattering of adsorbates at metal surfaces.

ACKNOWLEDGMENTS

This work was supported by the Sonderforschungbereich 450 of the Deutsche Forschungsgemeinschaft, Analysis and Control of Ultrafast Photoinduced Processes (Subproject C7).

[1] M. Hentschel, R. Kienberger, C. Spielmann, G. A. Reider, N. Milosevic, T. Brabek, P. Corkum, U. Heinzmann, M. Drescher, and F. Krausz, Nature (London) **414**, 509 (2001).
[2] R. Kienberger *et al.*, Science **297**, 1144 (2002).
[3] M. Drescher, R. Hentschel, M. Kienberger, M. Uibracker, V. Yakovlev, A. Scrinzi, T. Westerwalbesloh, U. Kleineberg, U. Heinzmann, and F. Krausz, Nature (London) **419**, 803 (2002).
[4] P. H. Bucksbaum, Nature (London) **421**, 593 (2003).
[5] G. G. Paulus, F. Lindner, H. Walther, A. Baltuska, E. Goulielmakis, M. Lezius, and F. Krausz, Phys. Rev. Lett. **91**, 253004 (2003).
[6] A. Föhlisch, P. Feulner, F. Hennies, D. Fink, A. Menzel, P. M. Sanchez-Portal, D. Echenique, and W. Wurth, Nature (London) **436**, 373 (2005).

[7] K. Kulander, Phys. Rev. A **36**, 2726 (1987).
[8] R. Grobe and J. H. Eberly, Phys. Rev. A **48**, 4664 (1993).
[9] M. S. Pindzola, P. Gavras, and T. W. Gorczyca, Phys. Rev. A **51**, 3999 (1995).
[10] H. Yu and A. Bandrauk, Phys. Rev. A **56**, 685 (1997).
[11] F. Remacle and R. Levine, J. Chem. Phys. **110**, 5089 (1999).
[12] F. Calvayrac, P.-G. Reinhard, E. Suraud, and C. Ullrich, Phys. Rep. **337**, 493 (2000).
[13] K. Harumiya, I. Kawata, H. Kono, and Y. Fujimura, J. Chem. Phys. **113**, 8953 (2000).
[14] J. Breidbach and L. Cederbaum, J. Chem. Phys. **118**, 3983 (2003).
[15] M. Suzuki and S. Mukamel, J. Chem. Phys. **119**, 4722 (2003).
[16] T. Klamroth, Phys. Rev. B **68**, 245421 (2003).
[17] S. Laulan and H. Bachau, Phys. Rev. A **68**, 013409 (2003).
[18] J. Zanghellini, M. Kitzler, C. Fabian, T. Brabec, and A. Scrinzi, Laser Phys. **13**, 1064 (2003).
[19] T. Kato and H. Kono, Chem. Phys. Lett. **392**, 533 (2004).
[20] X. Chu and S. I. Chu, Phys. Rev. A **70**, 061402(R) (2004).
[21] G. Paramonov, Chem. Phys. Lett. **411**, 350 (2005).
[22] T. Burnus, M. Marques, and E. Gross, Phys. Rev. A **71**, 010501(R) (2005).
[23] M. Nest, T. Klamroth, and P. Saalfrank, J. Chem. Phys. **122**, 124102 (2005).
[24] P. Krause, T. Klamroth, and P. Saalfrank, J. Chem. Phys. **123**, 074105 (2005).
[25] P. Krause, T. Klamroth, and P. Saalfrank, J. Chem. Phys. **127**, 034107 (2007).
[26] I. Barth and J. Manz, Angew. Chem. Int. Ed. **45**, 2962 (2006).
[27] I. Barth, J. Manz, Y. Shigeta, and K. Yagi, J. Am. Chem. Soc. **128**, 7043 (2006).
[28] T. Klamroth, J. Chem. Phys. **124**, 144310 (2006).
[29] A. Castro, M. Marques, H. Appel, M. Oliveira, C. Rozzi, X. Andrade, F. Lorenzen, E. Gross, and A. Rubio, Phys. Status Solidi B **243**, 2465 (2006).
[30] H. Schlegel, S. Smith, and X. Li, J. Chem. Phys. **126**, 244110 (2007).
[31] B. Schäfer-Bung and M. Nest, Phys. Rev. A **78**, 012512 (2008).
[32] J. Schmidt, E. Goulielmakis, and V. S. Yakovlev, J. Phys. B **41**, 115602 (2008).
[33] S. Klinkusch, T. Klamroth, and P. Saalfrank, Phys. Chem. Chem. Phys. **11**, 3875 (2009).
[34] S. Klinkusch, T. Klamroth, and P. Saalfrank, J. Chem. Phys. **131**, 114304 (2009).
[35] T. Klamroth and M. Nest, Phys. Chem. Chem. Phys. **11**, 349 (2009).
[36] M. Nest, Chem. Phys. Lett. **472**, 171 (2009).
[37] T. Kato and H. Kono, Chem. Phys. Lett. **392**, 533 (2004).
[38] J. C. Tremblay, T. Klamroth, and P. Saalfrank, J. Chem. Phys. **129**, 084302 (2008).
[39] G. Lindblad, Commun. Math. Phys. **48**, 119 (1976).
[40] V. Gorini, A. Kossakowski, and E. C. G. Sudarshan, J. Math. Phys. **17**, 821 (1976).
[41] V. Gorini and A. Kossakowski, J. Math. Phys. **17**, 1298 (1976).
[42] R. Kosloff, M. Ratner, and W. B. Davis, J. Chem. Phys. **106**, 7036 (1997).
[43] D. M. Lockwood, M. Ratner, and R. Kosloff, Chem. Phys. **268**, 55 (2001).
[44] E. A. Weiss, G. Katz, R. H. Goldsmith, M. R. Wasielewski, M. Ratner, R. Kosloff, and A. Nitzan, J. Chem. Phys. **124**, 074501 (2006).
[45] J. C. Tremblay and P. Saalfrank, Phys. Rev. A **78**, 063408 (2008).
[46] J. Olsen and P. Jørgensen, J. Chem. Phys. **82**, 3235 (1985).
[47] P. Craig and T. Thirunamachandran, *Molecular Quantum Electrodynamics* (Academic Press, New York, 1984).
[48] B. Gao, C. Pan, C.-R. Liu, and A. F. Starace, J. Opt. Soc. Am. B **7**, 622 (1990).
[49] M. Casida, C. Jamorski, K. Casida, and D. Salahub, J. Chem. Phys. **108**, 4439 (1998).
[50] B. J. Orr and J. F. Ward, Mol. Phys. **20**, 513 (1971).
[51] M. E. Casida, in *Recent Advances in Density Functional Methods*, edited by D. P. Chong (World Scientific, Singapore, 1995), Part I.
[52] M. E. Casida, *Recent Developments and Applications of Modern Density Functional Theory*, edited by J. M. Seminario (Elsevier, Amsterdam, 1996).
[53] P. Norman, D. M. Bishop, H. J. A. Jensen, and J. Oddershede, J. Chem. Phys. **115**, 10323 (2001).
[54] P. Norman, D. M. Bishop, H. J. A. Jensen, and J. Oddershede, J. Chem. Phys. **123**, 194103 (2005).
[55] A. J. Thorvaldsen, K. Ruud, K. Kristensen, P. Jørgensen, and S. Coriani, J. Chem. Phys. **129**, 214108 (2008).
[56] K. Kristensen, J. Kauczor, T. Kjærgaard, and P. Jørgensen, J. Chem. Phys. **131**, 044112 (2009).
[57] X. Blase and P. Ordejón, Phys. Rev. B **69**, 085111 (2004).
[58] L. Jensen, J. Autschbach, and G. C. Schatz, J. Chem. Phys. **122**, 224115 (2005).
[59] M. Head-Gordon, R. J. Rico, M. Oumi, and T. J. Lee, Chem. Phys. Lett. **219**, 21 (1994).
[60] W. H. Press, S. A. S. A. Teukolsky, W. T. Vetterling, and B. P. Flannery, *Numerical Recipes in FORTRAN 77 The Art of Scientific Programming* (Cambridge University Press, 1986).
[61] J. C. Tremblay and T. Carrington Jr., J. Chem. Phys. **121**, 11535 (2004).
[62] W. Kolos and L. Wolniewicz, J. Chem. Phys. **46**, 1426 (1967).
[63] G. A. Victor, J. C. Browne, and A. Dalgarno, Proc. Phys. Soc. **92**, 42 (1967).
[64] R. L. Wilkins and H. S. Taylor, J. Chem. Phys. **48**, 4934 (1968).
[65] G. A. Victor and A. Dalgarno, J. Chem. Phys. **50**, 2535 (1969).
[66] D. M. Bishop and L. M. Cheung, J. Chem. Phys. **72**, 5125 (1980).
[67] T. H. Dunning, J. Chem. Phys. **90**, 1007 (1989).
[68] A. K. Wilson, T. van Mourik, and T. H. Dunning, J. Mol. Struct. **388**, 339 (1996).